State Key Laboratory of Bioactive Substance and Function of Natural Medicines[1], Institute of Materia Medica, Chinese Academy of Medical Sciences and Peking Union Medical College, Beijing; College of Pharmacy[2], Jiamusi University, Jiamusi, China

Inhibiting the proliferation, migration and invasion of triple negative breast cancer cells through anti-tumor human serum albumin nanoparticles loading aziditaxel as a novel taxane derivative

Li-qing Chen[1,#], Zhe-ming Zhang[1,#], Wei Huang[1,*], Zhong-gao Gao[1,*], Wei-shuo Fang[1], Ming-ji Jin[1], Lian Yu[2]

Received August 31, 2016, accepted November 5, 2016

**Corresponding authors: Wei Huang, Zhong-gao Gao, State Key Laboratory of Bioactive Substance and Function of Natural Medicines, Institute of Materia Medica, Chinese Academy of Medical Sciences and Peking Union Medical College, 1 Xian Nong Tan Street, Beijing 100050, China*
huangwei@imm.ac.cn; zggao@imm.ac.cn
[#]These authors contributed equally to this work.

Pharmazie 72: 152–160 (2017) *doi: 10.1691/ph.2017.6146*

Triple negative breast cancer (TNBC) is a severe breast cancer subtype with the high mortality rate, and still is lack of effective therapeutic means so far. Aziditaxel, a water-insoluble compound, is a novel taxane derivative with strong anti-tumor activity. In this study, we constructed an aziditaxel-loaded nano drug delivery system using human serum albumin as a carrier, and further investigated its anti-tumor effect on TNBC *in vitro*. An emulsion solvent evaporation method was employed to prepare aziditaxel-loaded human serum albumin nanoparticles (AT-NPs). Their physicochemical properties were characterized according to morphology, particle size, zeta potential, reconstitution stability and *in vitro* drug release. The *in vitro* anti-tumor effects of AT-NPs on TNBC were evaluated using a 4T1 murine triple negative mammary cancer cell lines as the TNBC model. The results showed that AT-NPs could be effectively taken up by 4T1 cells in a time-dependent manner. Cell Counting Kit-8 assay showed that the IC_{50} of AT-NPs was 0.17 μg/ml. Meanwhile, compared with AT, AT-NPs had a better ability to promote apoptosis and induce G_2/M cycle arrest. On the other hand, AT-NPs had significantly inhibitory effects on the 4T1 cell adhesion, migration and invasion with the respective average inhibition ratios of 32.53%, 83.26% and 75.78%. Thus, our study revealed that AT-NPs had favorable antitumor activity *in vitro* and exhibited a good prospect for application in the field of TNBC therapy.

1. Introduction

Breast cancer ranks first in women cancer both in the developing and the developed world. Although some risk reduction might be achieved with prevention, those measures cannot eliminate the majority of breast cancers in low- and middle-income countries where breast cancer is diagnosed in very late stages (Anderson et al. 2015). Triple negative breast cancer (TNBC) refers to a special subtype of breast cancer characterized by the absence of the estrogen receptor (ER), the progesterone receptor (PR), and human epidermal growth factor receptor 2 (HER2) (Uematsu 2011; Bayraktar and Glück 2013). According to the statistic data in 2011, 20% of the 230480 breast cancer diagnosed cases were TNBC (Mahamodhossen et al. 2013; Swede et al. 2011). It is because of the lack of effective therapeutic targets that TNBC leads to the early clinical recurrence, poor prognosis, increased likelihood of distant recurrence and high mortality (Bonzanini et al. 2012; Fayaz et al. 2013; Dent et al. 2007; Caldarella et al. 2011). Of course, patients with TNBC have not been benefited from popular HER2-targeted monoclonal antibodies such as trastuzumab and pertuzumab. So far, there are still no standard treatment regimens for TNBC patients. Therefore, it is urgent to develop new therapeutic drugs for TNBC.

Aziditaxel (AT, coded as Lx2-32c, Figure1A), 2-debenzoyl-2-(3-azido-benzoyl)-7-prop-ionyl-10-deacetylcephalomannine, is a new taxane derivative which was obtained through semi-synthesis from cephalomannine by Prof. Fang's group in our institute (Xiao et al. 2011). AT is effective to some drug-resistant tumors because of its strong affinity to β-tubulin and thereby antagonising the efflux of P-glycoprotein (Zhou 2012), which is different from the well-known drugs paclitaxel and docetaxel. The results of pharmacodynamic and pharmacokinetic studies have shown that the compound's antitumor mechanism is similar to paclitaxel, but its ability of stabilizing microtubules is more powerful (Zhou 2012). AT can inhibit the growth of various tumor cells from different organizational sources *in vitro* (Wang et al. 2008a, b; Wang 2008; Zhou 2012; Zhou et al. 2012), such as Hela (human cervical carcinoma), KB (human oral epithelial carcinoma) and vincristin-resistant KB/V, A549 (human lung adenocarcinoma) and paclitaxel-resistant A549/T, BGC-803 (human gastric carcinoma), BGC-823 (human gastric carcinoma), MGC-803 (human gastric carcinoma) and paclitaxel-resistant BGC-823/T, Bel-7402 (human liver carcinoma) and fluorouracil-resistant Bel-7402/5-Fu, MX-1 (human breast carcinoma) and paclitaxel-resistant MX-1/T, MCF-7 (human breast carcinoma) and paclitaxel-resistant MCF-7/T, A2780 (human ovarian carcinoma). All IC_{50} values of the above cancer cells were less than 100 nM. Animal experiments exibited that AT could not only significantly inhibit the growth of Lewis lung cancer in mice, but also suppress the growth of A549, BGC-823, A2780, paclitaxel-resistant MX-1/T human cancer xenograft in nude mice (Wang et al. 2008a, b; Wang 2008; Zhou 2012; Zhou et al. 2012).

However, due to the similar chemical structure, AT has the same problem of poor solubility as paclitaxel, which impacts the drug efficacy and needs to be solved in a pharmaceutical way. For the past few years, nano drug delivery systems have been gradually catching more attentions due to its ability to increase the solubility of hydrophobic drugs and enhance tumor targeting (Kouchakzadeh et al. 2015). Recent researches are prone to study protein-based nanocarriers such as carriers based on serum albumin, transferrin and other endogenous proteins (Ding et al. 2014). Human serum albumin (HSA) is the most abundant protein in plasma and has been put into use as drug delivery carrier in the past 15-20 years. HSA

has many advantages such as good biocompatibility, stability, non-immunogenicity and ability to enhance the solubility of hydrophobic drugs. Albumin could be preferentially taken up by tumors as nutrition ingredient. Moreover, the gp-60 albumin receptor on vascular endothelia cells and secreted protein acidic rich in cysteine (SPARC) in the extracellular matrix (ECM) of tumor tissue endow albumin with the abilities to cross endothelial barrier to tumor and further inner tumor areas respectively (Neesse et al. 2014; Schnitzer and Oh 1992). The first approved case of HSA preparation, HSA-bound paclitaxel nanoparticle injection (Abraxane®) was employed to treat advanced (metastatic) breast cancer as monotherapy, advanced (metastatic) pancreatic cancer as first line treatment and advanced non-small cell lung cancer as combination therapy in clinical practice (Cecco et al. 2014). In summary, HSA can serve as a good carrier for preparing nano drug delivery systems for cancer treatment.

In view of AT's powerful antitumor efficacy, we tried to use AT to treat TNBC. In the present study, we used HSA as a carrier to construct the AT-loaded nano drug delivery system. AT-loaded HSA nanoparticles (AT-NPs) were prepared through the emulsion solvent evaporation method, and their physicochemical

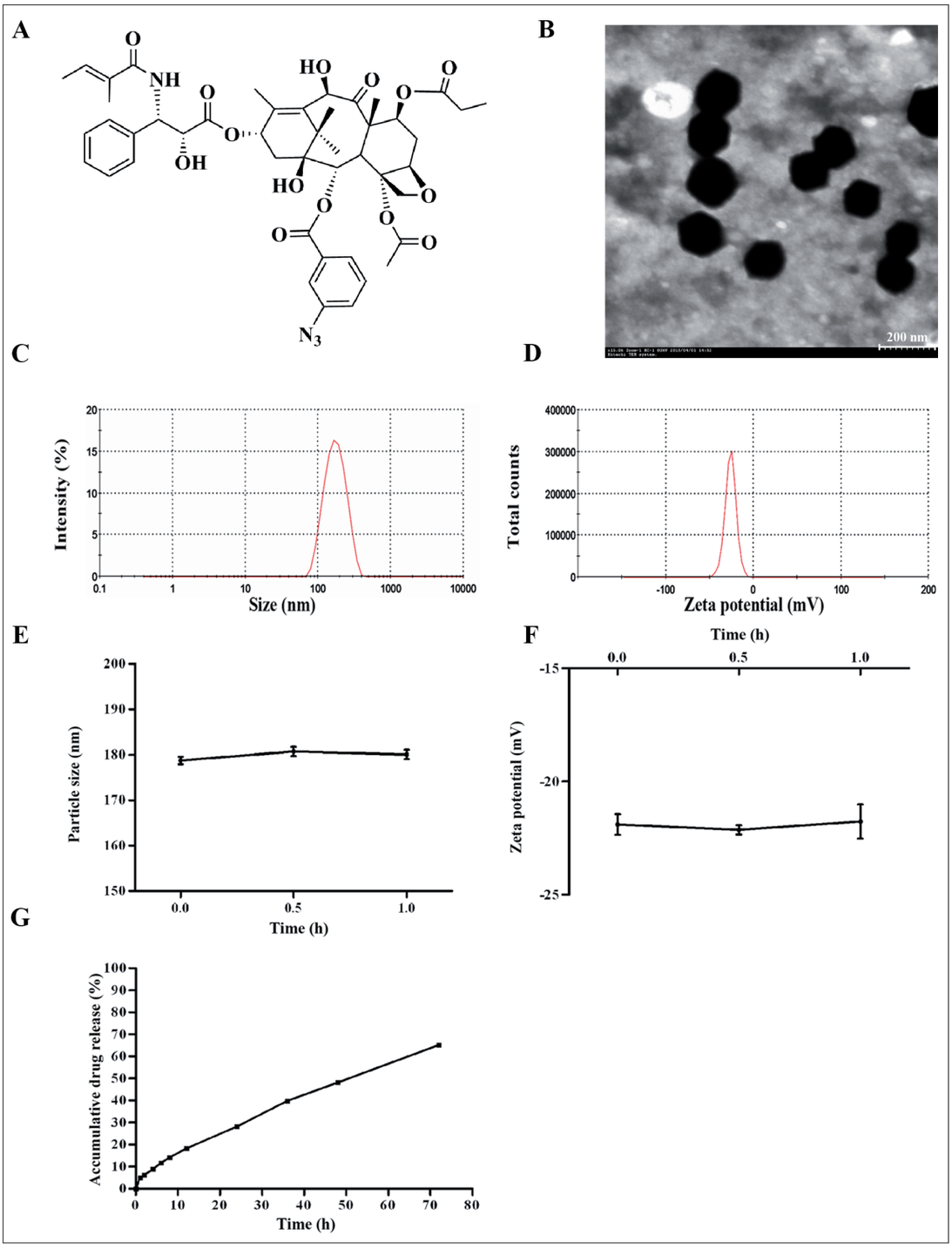

Fig. 1: (A) Chemical structure of AT molecule. (B) Morphology image of AT-NPs under the transmission electron. (C) Particle size distribution of AT-NPs. (D) Zeta potential distribution of AT-NPs. (E) Particle size changes over time of AT-NPs, mean ± SD (n=3). (F) Zeta potential changes over time of AT-NPs, mean ± SD (n=3). (G) In vitro drug release curve of AT-NPs in PBS.

Table 1: Within and between-day precision of the HPLC method

Concentration (μg/mL)	n	Within-day precision		Between-day precision	
		Mean	RSD(%)	Mean	RSD(%)
6.25	5	253.91	1.02	254.05	0.42
50.0	5	2061.72	0.55	2064.28	0.47
400.0	5	16160.66	0.65	16153.03	0.21

Table 2: Results of recovery experiments of the HPLC method

Level (%)	n	Concentration (μg/mL)	Amount recovered (μg/mL)	Recovery (%)	RSD (%)
80	3	40.0	39.31	98.28	1.40
100	3	50.0	50.23	100.46	0.72
120	3	60.0	60.66	101.10	1.13

properties were characterized in detail. Furthermore, we used the 4T1 mammary cancer cell line to evaluate the antitumor effect of AT-NPs, and the inhibitory effects of AT-NPs on 4T1 cell proliferation, adhesion, migration and invasion were investigated thoroughly. It has been reported that 4T1 mouse mammary tumor cell line, as a late stage (metastatic or advanced) breast cancer, is characterized as ER/PR/HER-2 negative, and more importantly it is one of only a few breast cancer models possessing the capacity to metastasize efficiently to sites similar to human breast cancer (Kaur et al. 2012; Tao et al. 2008). So, 4T1 cells were selected as the model system in the present study.

2. Investigations and results

2.1. Preparation and physicochemical characterization of AT-NPs

AT-NPs were prepared through the emulsion solvent evaporation method. Under transmission electron microscopy (TEM), it was observed that AT-NPs exhibited a sphere-like shape, and the particles were homogeneous in size (Fig. 1B). Further, the particle size, polydispersity index (PDI) and zeta potential AT-NPs were determined in a Zetasizer NanoZS analyzer. The assay results showed that the average size of AT-NPs was 165.8 nm (Fig. 1C), and PDI value was 0.102. This suggested that the particle size distribution of AT-NPs was in a narrow range and consistent with the above results of TEM observation. The zeta potential of AT-NPs was -26.1 mV (Fig. 1D), which suggested that there was a high density of negative charge on the particle surface of AT-NPs. The repulsion effect of congener charge among nanoparticles could contribute to the stability of an AT-NPs suspension system. In order to characterize the drug-loading capacity of AT-NPs, a HPLC quantitative method was developed to determine the AT content in AT-NPs. The standard curve established showed that AT peak area (A) presented a good linear relationship with the AT concentration (C) in the range of 6.25 μg/ml to 400 μg/ml. Through linear regression, the standard curve equation was obtained as follow: $A=40.457C+43.405$ ($R^2=0.9999$). Certainly, this HPLC method also was validated in view of precision and accuracy (Table 1 and Table 2) according to the International Conference on Harmonization(ICH) guideline Q2, which suggested that it was suitable for the accurate quantitation of AT in AT-NPs. The subsequent assay results showed that loading capacity (LC) of AT-NPs was 10.93%.

In order to check the reconstitution stability of AT-NPs, the lyophilized AT-NPs powder was reconstituted with 5% glucose injection to monitor the changes of particle size and zeta potential. It was found that the particle size (Fig. 1E) and zeta potential (Fig. 1F) did not exhibit remarkable changes compared with those of AT-NPs sample prior to lyophilization, which suggested that the freeze-drying operation had no significant influence on AT-NPs. In addition, the results showed that the reconstituted AT-NPs sample did not remarkably change in particle size and zeta potential within 1 h, which indicated that the reconstituted AT-NPs suspension remained stable and could meet the requirement of intravenous injection *in vivo*.

Drug release from AT-NPs was characterized in homotonic PBS solution (pH 7.4, containing 0.5% Tween-80) as the release medium. The accumulative drug release curve is presented in Fig. 1G. It was found that the drug accumulation release percentage reached over 65% after 72 h. It also was observed that AT-NPs released drug in a sustained-release pattern. Further, the *in vitro* release curve was mathematically related to various release models. The results are listed in Table 3. It was found that the drug release behavior of AT-NPs conformed to the Peppas-Sahlin sustained-release model ($R^2=0.999$).

2.2. Cellular uptake of AT-NPs

Coumarin-6 (C6) can generate green fluorescence under the condition of excitation at 466 nm, and so it is often used as a fluorescent probe in the tracer experiment (Rivolta et al. 2011). Here, C6 was used to label HSA nanoparticles to investigate the cellular uptake of nanoparticles in 4T1 cells through the fluorescent microscopy. The observation results were shown in Fig. 2. A weak green fluorescence could be seen in cells at the incubation time point of 15 min, which demonstrated that C6-labelled HSA nanoparticles (C6-NPs) could be quickly uptaken into 4T1 cells. With the incubation time increasing, the intensity of green fluorescence gradually enhanced, suggesting that the uptake amount of C6-NPs also gradually increased and reached a high uptake level at 2 h (Fig. 2). Generally, it was demonstrated that C6-NPs could be rapidly uptaken into 4T1 cells with high efficiency, which provided a strong support for AT-NPs to deliver AT into cells.

2.3. Inhibitory effect of AT-NPs on 4T1 cell proliferation

The inhibitory capacity of AT-NPs on the proliferation of 4T1 cells was investigated by Cell Counting Kit-8 (CCK-8) assay (Xu et al. 2015). The results are shown in Fig. 3A. It was found that AT-NPs could effectively inhibit the proliferation of 4T1 cells. The IC_{50} of AT-NPs on 4T1 cells was 0.17 μg/mL. Moreover, this inhibitory effect exhibited a dose-dependent pattern in the concentra-

Table 3: Fitting results of *in vitro* release curve of AT-NPs

Release model	Fitting equation	Fitting result	R^2
Zero order	$F=F_0+k_0*t$	F=5.407+0.875t	0.985
First order	F=100*[1-Exp(-k*t)]	F=100*[1-Exp(-0.015*t)]	0.984
Higuchi	$F=F_0+k*t^{0.5}$	F=-5.100 +7.652*t^0.5	0.977
Korsmeyer-Peppas	$F=F_0+k*t^n$	F= 3.273 *t^0.697	0.998
Hixson-Crowell	F=100*[1-(1-k*t)^3]	F=100*[1-(1-0.004*t)^3]	0.977
Peppas-Sahlin	$F=k_1*t^{0.5}+k_2*t$	F=3.632 *t^0.5+0.479 *t	0.999
Weibull	F=100*{1-Exp[-(t^β)/α]}	F=100*{1-Exp[-(t^0.868)/42.194]}	0.991

Data rounding: down to the third decimal point.

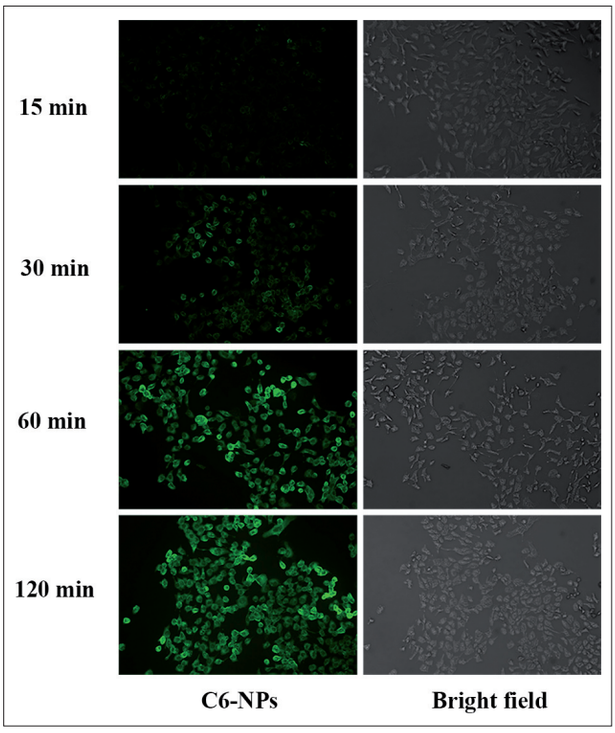

Fig. 2: Fluorescent microscopic images of 4T1 cells after incubation with C6-NPs for 15 min, 30 min, 60 min and 120 min, respectively.

tion range of 0.01 μg/ml to 10 μg/ml. With the AT concentration increasing, the cell viability gradually decreased, which suggested that the inhibitory capacity of AT-NPs on the 4T1 cell proliferation also gradually enhanced. The inhibition ratio of cell proliferation reached about 78% at the concentration of 10 μg/ml. On the other hand, the results (Fig. 3B) also showed that the inhibitory effect of AT-NPs on 4T1 cell proliferation was significantly stronger than that of AT itself at the concentration level of 1 μg/ml (**$p < 0.01$ for 48 h incubation, ***$p < 0.001$ for 24 h incubation).

2.4. Influence of AT-NPs on 4T1 cell apoptosis

Hoechst staining assay was conducted to detect the occurrence of 4T1 cells apoptosis induced by AT-NPs. The results are shown in Fig. 4. In the Hoechst staining assay, the nuclei of normal cells were regular shaped or elliptic and emitted dispersive blue fluorescence under the fluorescence microscope. When cell apoptosis happened, dense stained particles were seen in the nuclei or cytoplasm (Srivastava et al. 2015). Some 4T1 cells nuclei became broken and aggregated in both AT-NPs and AT groups (Fig. 4), which suggested that cell apoptosis happened in cells both groups. So, it was demonstrated that AT-NPs could effectively deliver and release AT to induce the apoptosis of 4T1 cells.

Subsequently, Annexin V-FITC/PI double staining assay was carried out to quantitatively determine the cell apoptosis by flow cytometry. The results are shown in Fig. 5. It was found that both AT-NPs and AT could induce remarkably cell apoptosis compared with the control group. However, the percentage of apoptotic cells (late apoptosis plus early apoptosis) in the AT-NPs group was 43.46% while it was only 16.38% in the AT group.

2.5. Influence of AT-NPs on 4T1 cell cycle

The influence of AT-NPs on 4T1 cell cycle was investigated by flow cytometry. The results are shown in Fig. 6. Compared with control group, it was found that both AT-NPs and AT could arrest 4T1 cell cycle at the phase of G_2/M and further induce the formation of polyploidy, which led to the proliferation inhibition of 4T1 cells. This suggested that AT-NPs could effectively deliver and release AT to arrest 4T1 cell cycle at G_2/M and sequentially inhibit cell proliferation. Additionally, the ratio of induced polyploidy in the AT-NPs group was 60.99% while it was 55.54% in the AT group.

2.6. Inhibitory effect of AT-NPs on 4T1 cell adhesion

The influence of AT-NPs on 4T1 cell adhesion was investigated by a matrigel-based adhesion assay (Chen et al. 2014). The results are shown in Fig. 7. It was found that the adhesion ratios of AT-NPs and AT were both significantly lower than in the control group, which suggested that both AT-NPs and AT could decrease the adhesion ability of 4T1 cells. In addition, the adhesion ratio in the AT-NPs group (67.47%±5.43%) was lower than that in the AT group (84.23%%±1.90%) (**$p < 0.01$), which indicated that the ability of AT-NPs to inhibit 4T1 cell adhesion was stronger than that of AT itself (Fig. 7).

2.7. Inhibitory effect of AT-NPs on 4T1 cell migration

The effect of AT-NPs on 4T1 cell migration was evaluated by qualitative observation and quantitative determination using the Transwell cell culture system (Wang et al. 2015). The results are shown in Fig. 8. The qualitative results showed that AT-NPs and AT could both inhibit the cell migration *in vitro*, and the inhibitory ability of AT-NPs was stronger than that of AT under the microscope (Fig. 8A). Quantitative results (shown in Fig. 8B) were consistent with the qualitative result. At the concentration level of 1 μg/ml, the migration ratios of 4T1 cells in AT-NPs and AT groups decreased to 16.74%±3.44% and 32.62%±6.19% respectively, which also demonstrated that AT-NPs could inhibit cell migration *in vitro* more effectively than AT itself (*$p < 0.05$).

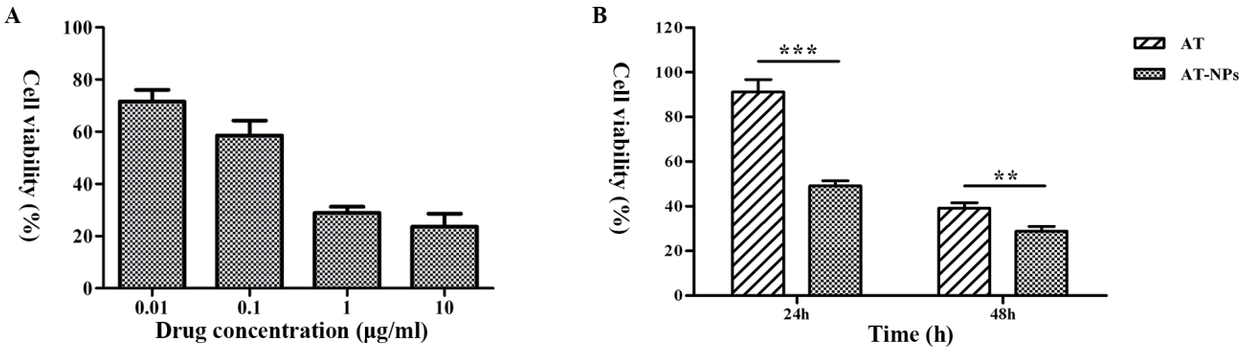

Fig. 3: Inhibitory effect of AT-NPs and AT on the proliferation of 4T1 cells. The data are shown as the mean ± SD (n=4). (A) Proliferation inhibition of AT-NPs on 4T1 cells after incubation for 48 h at different drug concentrations of 0.01, 0.1, 1, 10 μg/ml. (B) Proliferation inhibition of AT-NPs and AT on 4T1 cells after incubation for 24 h and 48 h, respectively. **$p < 0.01$, ***$p < 0.001$.

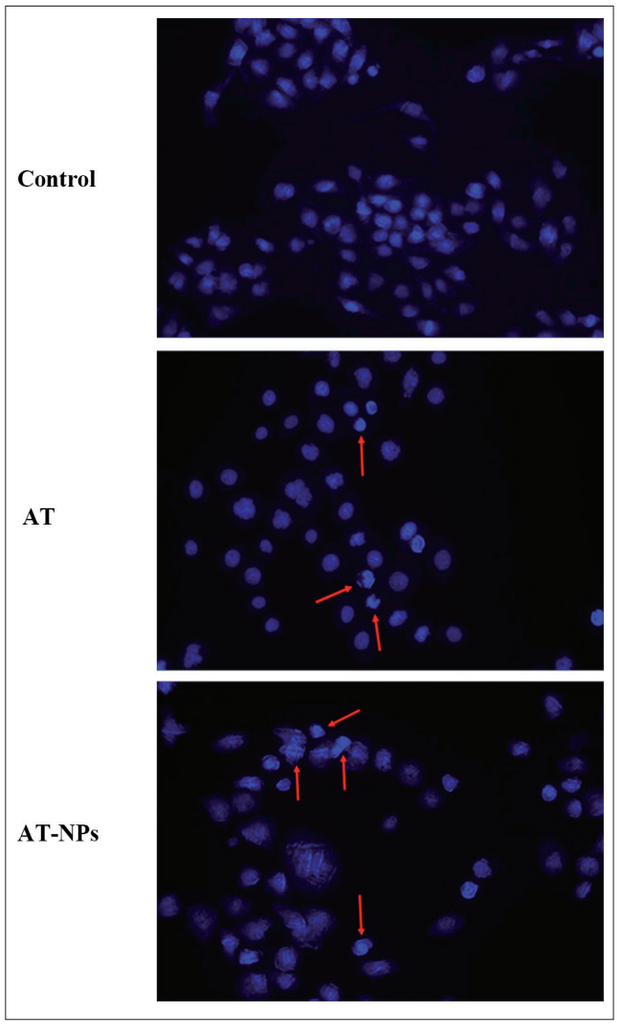

Fig. 4: Hoechst 33258 staining assay of 4T1 cells incubated respectively with AT-NPs and AT for 24 h at the drug concentration of 1 μg/ml. Red arrows indicate the apoptotic bodies.

2.8. Inhibitory effect of AT-NPs on 4T1 cell invasion

Similarily, the inhibitory effect of AT-NPs on 4T1 cell invasion was also investigated through qualitative observation and quantitative assay. The results are shown in Fig. 9. Under the microscope, it was observed that AT-NPs and AT could both effectively inhibit the invasion of 4T1 cells *in vitro*, and the inhibitory effect of AT-NPs was remarkably stronger than that of AT (Fig. 9A). The quantitative data demonstrated that the invasion ratio of 4T1 cells in AT-NPs and AT groups respectively decreased to 24.22%±0.27% and 31.25%±2.58% at the concentration of 1 μg/ml, which also suggested that AT-NPs could more effectively inhibit the cell invasion *in vitro* than AT (*$p < 0.05$) (Fig. 9B). Also, this was consistent with the above qualitative results.

3. Discussion

Although AT can be dissolved in a solvent mixture of Cremophor EL (polyoxyethylated castor oil) and ethanol (1:1, v/v) to prepare a conventional injection referred to commercial Taxol®, several drawbacks are encountered in the clinical use of Cremophor EL. The most common are anaphylactic hypersensitivity reactions, neurotoxicity, hyperlipidemia, and so on. In addition, it could dissolve divinyl hexyl phthalates in the polyvinyl chloride infusion sets and alter the pharmacokinetics and pharmacodynamic profiles of paclitaxel (Gelderblom et al. 2001; van Zuylen et al. 2001; Waugh et al. 1991). Recently, a Cremophor-free paclitaxel injection, Abraxane®, has been developed, a paclitaxel-loaded human serum albumin nanoparticles suspension prepared by NAB technology (Ibrahim et al. 2002; Gradishar 2006). The preparation process can maintain the biological properties of HSA and combine the molecule of HSA with paclitaxel, which solves the poor solubility problem of paclitaxel and avoids the side effect caused by the oily solvent Cremophor. AT is similar to paclitaxel in chemical structure and also has poor solubility in water. Accordingly, we followed the idea of Abraxane® and prepared AT-NPs using HSA. There are many methods to prepare serum albumin nanoparticles, such as the adsorption equilibrium method (Dreis et al. 2007), the desolvation and/or crossing link method(Bae et al. 2012; Wartlick et al. 2004), and the emulsion solvent evaporation method(Wan et al. 2015). As we all know, Abraxane® employed the emulsion solvent evaporation method. Compared with the other two methods, emulsion solvent evaporation is simple, stable, without organic solvent and has good repeatability, and could be enlarged for industrial production. In this study, the prepared AT-NPs possessed moderate size, high drug loading capacity, fine reconstitution stability and sustained-release pattern, which indicated that AT has good compatibility with HSA and HSA-bound nanoparticle was a good choice for AT preparations.

AT is a new taxane derivative. Previous researches focus on the mechanism or pharmacodynamics study of AT. There exist only two preparations of AT which have been investigated in detail: Lx2-32c-loaded polymeric micelles (Chen et al. 2016) and Lx2-32c-containing liposomes (Wang et al. 2014). AT-NPs were firstly prepared in our study. Abraxane® has exhibited significant benefits in treatment of metastatic breast cancer. Generally, the poor prognosis of TNBC was associated with the tumor metastasis of lung (Aslakson and Miller 1992), brain (Kodack et al. 2015), bone (Azim et al. 2012) lymph nodes and other organs (Abreu et al. 2014), and there is a peak of metastasis occurring after one year (Bayraktar and Glück 2013). In tumor metastasis, the tumor cells need to change their motility and become invasive (Fidler 2003). Several discrete steps are discernable in the biological cascade of metastasis: adhesion to the ECM, secretion of matrix-degrading enzymes such as matrix metalloproteinases (MMPs), increased motility and invasiveness, entry and survival in the circulation, exit into new tissue, and eventual colonization of a distant site (Gupta and Massagué 2006). It has been proven that one of effective means against tumor metastasis is inhibiting the adhesion, migration and invasion of tumor cells (Gupta and Massagué 2006). Also, previous molecular detection illustrated that AT itself could significantly block the secretions of MMPs in MDA-MB-231cells, HTl080 cells and A375 cells (Zhou 2012). Additionally, AT displayed impressive activity in anti-angiogenesis in an *in vitro* tube forming assay (Zhou 2012). The above results suggested that AT may perform well in fighting tumor metastasis. Therefore, we investigated the inhibitory effect of AT-NPs on the adhesion, migration and invasion on 4T1 triple negative breast cancer cells in order to verify the anti-metastasis activities of AT-NPs compared with AT. We used matrigel and Transwell chambers to simulate ECM and epithelial cell basement membrane (BM), respectively. Our results demonstrated that AT-NPs exhibited a significant inhibitory effect on the adhesion, migration and invasion of 4T1 cells, and so it was accordingly suggested that AT-NPs might play an inhibitory effect on the TNBC metastasis *in vivo*.

In summary, we have successfully developed AT-NPs with good physicochemical properties and evaluated their antitumor activity *in vitro* using 4T1 triple negative breast cancer cells. AT-NPs demonstrated more effective impact on the proliferation, apoptosis, and G_2/M cycle arrest of 4T1 cancer cells *in vitro* than AT. More importantly, AT-NPs significantly inhibited tumor adhesion, migration and invasion on highly metastatic 4T1 cells. Thus, our study revealed that AT-NPs had favorable antitumor activity *in vitro* and exhibited a good prospect for application in the field of TNBC therapy.

4. Experimental

4.1. Materials

AT (Lot. 32C-140114, purity 99.8%) was provided as a gift by Prof. Weishuo Fang from Institute of Materia Medica, Chinese Academy of Medical Science & Peking Union Medical Collage. Human serum albumin and Coumarin-6 was bought from SIGMA-

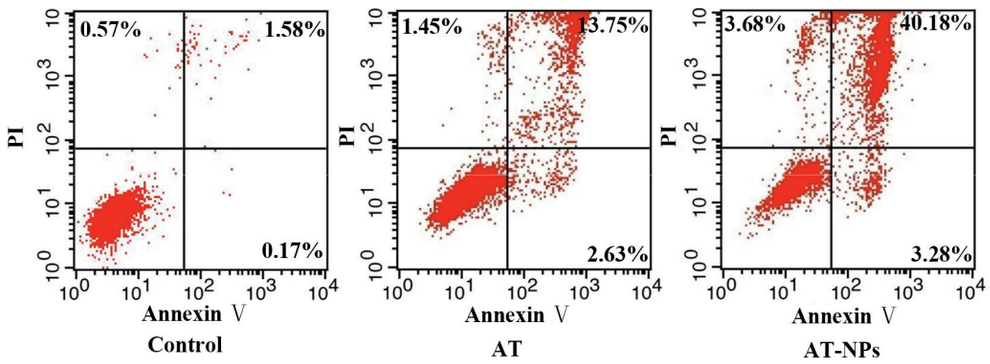

Fig. 5: Annexin V-FITC/PI double staining assay of 4T1 cells incubated respectively with AT-NPs and AT for 48 h at the drug concentration of 1 μg/ml through flow cytometry.

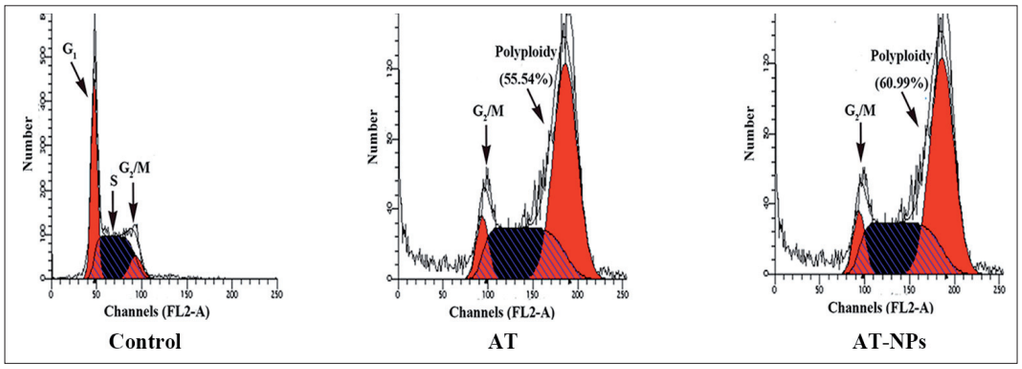

Fig. 6: Cell cycle assay of 4T1 cells incubated respectively with AT-NPs and AT for 24 h at the drug concentration of 1 μg/ml.

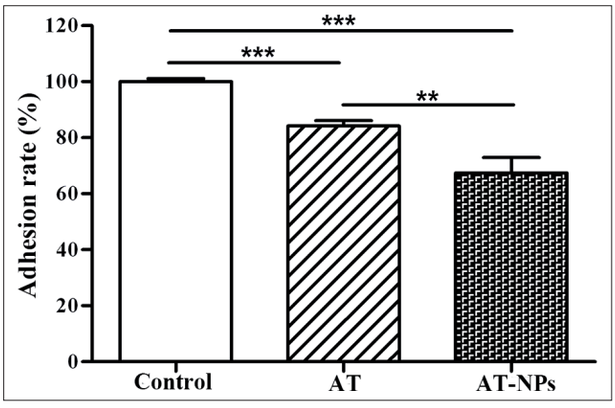

Fig. 7: Quantitative determination of 4T1 cell adhesion ratio after respective incubation with AT-NPs and AT for 60 min at the drug concentration of 1 μg/ml. The data are shown as the mean ± SD (n=3). **p < 0.01, ***p <0.001.

ALDRICH Company (St. Louis, USA). (USA). Cell Counting Kit-8 was purchased from DOJINDO Molecular Technologies, Inc. (Shanghai, China). Annexin V-FITC/PI Kit was obtained from KeyGEN BioTECH company (Nanjing, China). Matrigel and Transwell chambers were bought from Corning Incorporated (NY, USA). Crystal violet staining solution was purchased from Beijing Solarbio Science & Technology Co., Ltd (Beijing, China). Fetal bovine serum was supplied by Shanghai ExCell Biology Inc (Shanghai, China). RPMI 1640 medium, 0.25% trypsin-0.53 mM EDTA solution and PBS were all purchased from Thermo Fisher Scientific Inc (Walthan, USA). All other chemicals were of analytical grade and used without further purification.

4.2. Preparation of AT-NPs

We used the emulsion solvent evaporation method to prepare AT-NPs (Wan et al. 2015). Firstly, AT was dissolved in a mixed solvent of chloroform and ethanol (11:1, v/v). The AT solution was added into the 30 ml of HSA solution (10 mg/ml) under high shear state for 5 min to get the coarse emulsion. Further, the coarse emulsion was passed through a micro fluidizer (Nano DeBEE, USA) for 12-13 cycles at a pressure of 100-170 MPa to obtain the AT-NPs suspension, and then AT-NPs suspension was quickly evaporated for approximately 15 min by a rotary evaporator (ZX98, Shanghai) in order to remove the organic solvent. Then AT-NPs suspension was further filtered through filter membranes (Millipore, 220 nm pore diameter). Finally, the AT-NPs suspension was frozen at -80 °C and then lyophilized (Chirist Alpha 1-2/LD-Plus, Germany) for 48 h to get the AT-NPs lyophilized powder.

4.3. Morphology of AT-NPs

AT-NPs lyophilized powder was dissolved in deionized water and diluted to a concentration of 2 mg/ml. Then, AT-NPs suspension was dropped in the copper net and placed for 5 min. After being stained with 1% phosphotungstic acid solution for 5 min, AT-NPs sample was dried and observed under TEM (Hitachi H-7650, Japan).

4.4. Particle size and zeta potential of AT-NPs

Lyophilized AT-NPs powder was dissolved in deionized water and diluted to a concentration of about 0.1 mg/ml. Particle size, polydispersity index (PDI) and zeta potential of AT-NPs were determined by dynamic light scattering and electrophoretic light scattering through using a Malvern Zetasizer (NanoZS 90, UK).

4.5. Drug-loading capacity of AT-NPs

Drug-loading capacity (LC) of AT-NPs was measured by a HPLC analysis system (Agilent 1200, USA). HPLC analysis was carried out using the CuroSil-PFP column (Phenomenex, 250 × 4.6 mm, 5 μm) and a mixed solution of acetonitrile and water (45:55, v/v) as the mobile phase with a flow rate of 1.0 ml/min at 30 °C. AT was detected at a wavelength of 218 nm, and the wavelength of 360 nm was taken as a reference. The injection volume was 20 μl. The 20 mg AT powder was weighed precisely and dissolved in the 25 ml of methanol to obtain the AT stock solution at a concentration of 0.8 mg/ml. AT stock solution was respectively diluted to various concentrations of 6.25, 12.5, 25, 50, 100, 200, 400 μg/ml using the mobile phase, and all these solutions were subjected to HPLC detection under the above assay conditions. The standard curve was obtained through a linear regression between the concentration (C) as a dependent variable and the peak area (A) as an independent variable. The HPLC method was validated by a series of evaluations including the precision, accuracy according to ICH guideline Q2. Subsequently, the lyophilized AT-NPs powders were weighed precisely, and the weight was denoted by W_0. After being dissolved with the de-ionized water and diluted for three times by ethanol, AT-NPs suspension was subjected to ultrasound for

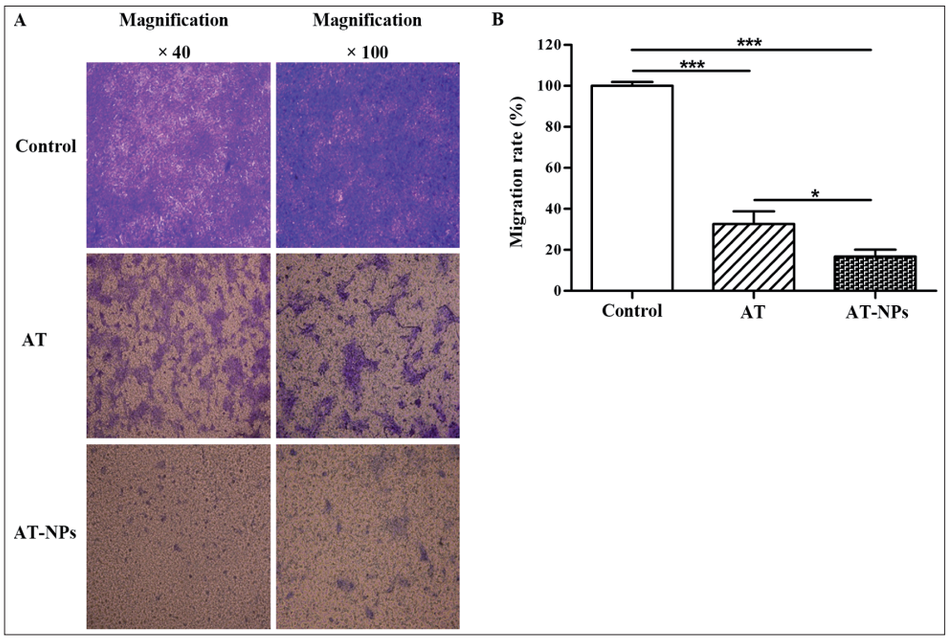

Fig. 8: Inhibition of AT-NPs and AT on the cell migration of 4T1 cells at the drug concentration of 1 μg/ml. (A) Images of crystal violet staining of transwell chambers membranes after respective incubation with AT-NPs and AT for 24 h. (B) Quantitative determination of 4T1 cell migration inhibition ratios after respective incubation with AT-NPs and AT for 24 h. The data are shown as the mean ± SD (n=3). *p < 0.05, ***p < 0.001.

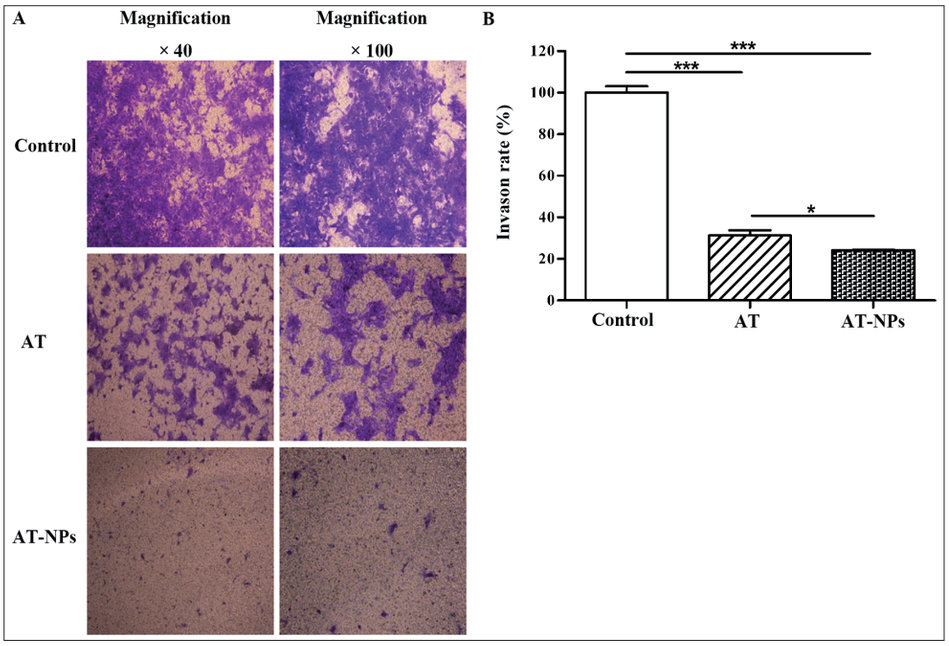

Fig. 9: Inhibitory effect of AT-NPs and AT on the cell invasion of 4T1 cells at the drug concentration of 1 μg/ml. (A) Crystal violet staining images of transwell chambers membranes after respective incubation with AT-NPs and AT for 24 h. (B) Cell invasion ratios of AT-NPs and AT after respective incubation with AT-NPs and AT for 24 h. The data are shown as the mean ± SD (n=3). *p <0.05, ***p<0.001.

10 min and then was centrifuged at a speed of 10000 × g for 10 min. Subsequently, the supernatant was collected to determine the concentration of AT through the above mentioned HPLC method. Finally, the weight of AT encapsulated in AT-NPs was calculated and denoted as W_1. Loading capacity (LC) was calculated according to the formula below.

$LC\ (\%) = W_1/W_0 \times 100$

4.6. Reconstitution stability

Lyophilized AT-NPs were dissolved in the 5% dextrose injection at a concentration of 5 mg/ml. After standing for 0 h, 0.5 h and 1 h at room temperature, 200 μl of AT-NPs suspension was taken out and diluted to appropriate concentration. Size, and zeta potential were determined to evaluate the reconstitution stability of AT-NPs.

4.7. In vitro release

Lyophilized AT-NPs were dissolved in the homotonic PBS solution (pH 7.4, containing 0.5% Tween-80) as the release medium at a concentration of 3 mg/ml. Then, 0.5 ml of AT-NPs suspension was transferred to a dialysis bag (MWCO 10 kDa), and the dialysis bag was put in the 40 ml of in a triangular flask at 37 °C and was shaken at 100 rpm. At each time point for detection, 0.2 ml of release medium was taken out and the same volume of fresh release medium was supplemented at the same time. After 72 h incubation, the dialysis bag was cut broken and the accumulative drug content at this

moment was regarded as the total drug amount. The obtained 0.2 ml release medium was centrifuged at 10000 × g for 10 min, and the supernatant was collected to determine the concentration of AT through the above established HPLC method. The amount of released AT was calculated, and then the accumulation release percent was calculated by dividing the accumulative release amount at the each time point by the total drug amount.

4.8. Cell culture

Murine triple negative mammary cancer cell line, 4T1, was purchased from Cell Bank in Chinese Academy of Sciences. The 4T1 cell line was cultured with RPMI 1640 medium containing 10% fetal bovine serum at 37 °C and 5% CO_2. 4T1 cells in the logarithmic growth phase were used in the following cell experiments.

4.9. Cellular uptake

In order to investigate *in vitro* cellular uptake of nanoparticles by 4T1 cells, C6 was chosen as the fluorescent probe to prepare the C6-NPs. C6-NPs were prepared using the same method except that coumarin-6 instead of AT was added to the chloroform and ethanol solvent before emulsification, and the C6-NPs were run over a sepharose CL-4B column to remove the free coumarin-6. 4T1 was seeded at a density of 2×10^4 cells/well in a 24-well plate and cultured at 37 °C and 5% CO_2 for 24 h. Then, cells were incubated with C6-NPs at 1 μg/ml at 37 °C for 15 min, 30 min, 60 min and 120 min, respectively. At the end of the incubation, cells were washed with the cold PBS for three times to remove the nanoparticles adhered on cell surfaces. Finally, cells were fixed with 4% paraformaldehyde solution in dark place and then observed under a fluorescent microscope (Olympus IX51, Japan).

4.10. In vitro cytotoxicity assay

In vitro cytotoxicity of AT-NPs against 4T1 cells was evaluated by CCK-8 assay. Briefly, 4T1 was seeded at 4×10^3 cells/well in a 96-well plate and cultured at 37 °C and 5% CO_2 for 24 h. AT-NPs suspension at different concentrations of 0.01, 0.1, 1, 10 μg/ml was respectively added to cells and incubated for 48 h. Meanwhile, AT-NPs suspension and AT solution at concentrations of 1μg/ml were respectively added to cells and incubated for 24 h or 48 h. Then, the culture media were replaced with 200 μl of fresh medium containing 10% CCK-8 reagent. After incubation for 2 h, the optical density (OD) values at 450 nm were measured through a microplate reader (BioTek Synergy H1, USA). Finally, cell viability was calculated according to the formula below. IC_{50} was calculated by Graphpad Prism software (version 5.0.0.0, GraphPad Software Inc., USA).

Cell viability (%) = $(OD_{test} - OD_{blank}) / (OD_{control} - OD_{blank}) \times 100$

4.11. Hoechst staining assay

Hoechst staining assay was introduced for the qualitative determination of apoptosis. In short, 4T1 cells were seeded at 5×10^4 cells/well in a 12-well plate and then incubated at 37 °C and 5% CO_2 for 24 h. After washing with PBS once, cells were incubated with the medium containing AT or AT-NPs at the 1 μg/ml of AT for 24 h. Additionally, the same volume of fresh medium without drug was used as a negative control. When the culture ended, cells were washed with PBS for three times and fixed by 4% paraformaldehyde for 15 min. Then, 10 μg/ml of Hoechst 33258 was used to stain the cell nuclei. Finally, the samples were washed three times with cold PBS and observed under a fluorescent microscope.

4.12. Annexin V-FITC/PI double staining assay

Quantitative determination of the apoptotic percentage of AT-NPs was conducted by Annexin V-FITC/PI double staining assay. 4T1 cells were seeded at a density of 7×10^4 cells/well in a 12-well plate and cultured at 37 °C and 5% CO_2 for 24 h. After washing with PBS one time, cells were respectively incubated with the medium containing AT and AT-NPs at the 1 μg/ml of AT for 48 h. Subsequently, cells were collected and washed twice with PBS, and then were mixed with 500 μl combining solution, 5 μl Annexin V-FITC and 5 μl PI to stain for 15 min at room temperature. All the staining operations needed to be protected from light. Finally, the samples were detected and analyzed by flow cytometry (BD FACSAria, USA).

4.13. Cell cycle assay

In order to investigate the cell cycle arrest effect of AT-NPs, 4T1 cells were seeded in a 6-well plate at a density of 2×10^5 cells/well and cultured at 37 °C and 5% CO_2 for 24 h. Then, cells were incubated with the medium containing AT and AT-NPs at 1 μg/ml of AT for another 24 h. Then, cells were trypsinized by 0.25% trypsin and centrifuged at 400 × g for 4 min to collect. After cell samples were fixed by 70% ethanol at -20 °C for 24 h, cells were re-suspended in 1 ml PBS and mixed with RNase to incubate at 37 °C for 30 min. Finally, cell samples were stained by PI staining solution (50 μg/ml) for 1 h, and then were detected and analyzed by flow cytometry.

4.14. Cell adhesion assay

Matrigel (50 mg/ml) was diluted with serum-free RPMI-1640 medium at a ratio of 1:5 and added into wells of a 96-well plate, and the plate was incubated at 37 °C and 5% CO_2 overnight for matrigel concreting. Then, the matrigel was hydrated and washed with serum-free medium. The 4T1 cells were trypsinized for collection and re-suspended at a density of 5×10^5 cells/ml. The cell suspensions were added into wells of the above matrigel-coated plate at a volume of 100 μl/well. Then, the cell suspensions were mixed with AT or AT-NPs at a 1 μg/ml of AT to incubate for 60 min at 37 °C and 5% CO_2. After incubation, the media in the plate wells were discarded, and the matrigel was washed with PBS. The cells on the matrigel were subjected to MTT assay, and the optical density (OD) values at 450 nm were measured with a microplate reader (BioTek, USA). Finally, cell adhesion ratios were calculated according to the below formula.

Adhesion ratio (%) = $(OD_{test} - OD_{blank}) / (OD_{control} - OD_{blank}) \times 100$

4.15. Cell migration assay

The 24-well Transwell plate containing insert with 8 μm pore size membrane was used to evaluate the migration and invasion of tumor cells. In cell migration assay, 4T1 cells were collected and washed with PBS, and then were re-suspended with serum-free RPMI-1640 medium at a density of 2×10^6 cells/ml. The cells were mixed with AT or AT-NPs at 1 μg/ml of AT. Also, we set a negative control group in which the cells suspension was mixed with serum-free RPMI-1640 medium without drug. 100 μl of the cells suspensions in different groups were seeded in the upper insert chamber, and 600 μl of RPMI 1640 medium with 10% FBS were added in each lower well chamber. After cell culture at 37 °C and 5% CO_2 for 24 h, the chamber inserts were washed with PBS and then fixed by cold methyl alcohol at -20 °C for 10 min. The upper surface of chamber inserts was cleaned, and the chamber inserts were air-dried. Then, these chamber inserts were stained with 500 μl 10% crystal violet in a new 24-well plate for 30 min. The chamber inserts were observed under a microscope and photos were taken in the different view fields. Finally, the crystal violet dye from the membrane of insert chamber were eluted with 33% acetic acid and detected by a microplate reader at 570 nm for quantitative test.

4.16. Cell invasion assay

Matrigel, which was diluted by serum-free RPMI-1640 medium, was added in transwell chamber inserts in a 24-well plate at a volume of 60 μl/well, and then were incubated at 37 °C and 5% CO_2 overnight. After incubation, the matrigel in the chamber inserts was hydrated and washed with serum-free medium. Subsequently, 4T1 cells were collected and re-suspended with serum-free RPMI-1640 medium at a density of 2×10^6 cells/ml. The cell suspensions were mixed with AT or AT-NPs at 1 μg/ml of AT and 100 μl of the cell suspensions was added in the upper insert chamber, and then 600 μl of the medium with 10% FBS was added in the lower well chamber. Also, a negative control was set at the same time. Cells were cultured at 37 °C and 5% CO_2 for 24 h. Then, the chamber inserts were fixed by cold methyl alcohol for 20 min at -20 °C. The matrigel coated on the upper surface of the chamber inserts was wiped off, and the chamber inserts were washed with PBS for three rimes and then air-dried. The chamber inserts were stained with crystal violet and taken photos under the microscope. For the qualitative test, the crystal violet dye from the membrane of insert chamber were eluted with 33% acetic acid and detected through a microplate reader at 570 nm.

4.17. Statistical analysis

The release curve of AT-PMs was fitted by DDSolver software (Zhang et al. 2010). Representative results are presented and expressed as mean±SD. Statistical analysis was conducted using the SPSS Statistics 19 (version 4.0.100.1124; SPSS Inc., IBM Company, USA). Statistical comparisons were performed to determine group difference through ANOVA (analysis of variance). Significant difference between two groups was evaluated by Student's t test. Asterisks indicate statistical significance as follows: * $p < 0.05$; ** $p < 0.01$; *** $p < 0.001$. All calculated data of results were rounded to the second decimal point except as specially provided.

Acknowledgements: This work was financially supported by National Natural Science Foundation of China (81373342, 81274101), Beijing Natural Science Foundation (2141004, 7142114) and Basic Research Program in State Key Laboratory of Bioactive Substance and Function of Natural Medicines.

Conflicts of interest: None declared.

References

Aslakson CJ, Miller FR (1992) Selective events in the metastatic process defined by analysis of the sequential dissemination of subpopulations of a mouse mammary tumor. Cancer Res 52: 1399–1405.

Azim HA, Kamal NS, Azim HA Jr (2012) Bone metastasis in breast cancer: the story of RANK-ligand. J Egypt Natl Canc Inst 24: 107-114.

Abreu EB, Martinez P, Betancourt L, Romero G, Godoy A, Bergamo L (2014) Treatment plan for breast cancer with sentinel node metastasis. Ecancermedicalscience 8: 383.

Anderson BO, Ilbawi AM, El Saghir NS (2015) Breast cancer in low and middle income countries (LMICs): a shifting tide in global health. Breast J 21: 111-118.

Bae S, Ma K, Kim TH, Lee ES, Oh KT, Park ES, Lee KC, Youn YS (2012) Doxorubicin-loaded human serum albumin nanoparticles surface-modified with TNF-related apoptosis-inducing ligand and transferrin for targeting multiple tumor types. Biomaterials 33: 1536–1546.

Bonzanini M, Morelli L, Bonandini EM, Leonardi E, Pertile R, Palma PD (2012) Cytologic features of triple-negative breast carcinoma. Cancer Cytopathol 120: 401-409.

Bayraktar S, Glück S (2013) Molecularly targeted therapies for metastatic triple-negative breast cancer. Breast Cancer Res Treat 138: 21-35.

Caldarella A, Crocetti E, Bianchi S, Vezzosi V, Urso C, Biancalani M, Zappa M (2011) Female breast cancer status according to ER, PR and H&ER2 expression: a population based analysis. Pathol Oncol Res 17: 753-758.

Cecco S, Aliberti M, Baldo P, Giacomin E, Leone R (2014) Safety and efficacy evaluation of albumin-bound paclitaxel. Expert Opin Drug Saf 13: 511-520.

Chen Y, Li Z, He Y, Shang DD, Pan JG, Wang HM, Chen HM, Zhu ZX, Wan L, Wang XD (2014) Estrogen and pure antiestrogen fulvestrant (ICI 182 780) augment cell-

matrigel adhesion of MCF-7 breast cancercells through a novel G protein coupled estrogen receptor (GPR30)-to-calpain signaling axis. Toxicol Appl Pharmacol 275: 176-181.

Chen LQ, Huang W, Gao ZG, Fang WS, Jin MJ (2016) lx2-32c–loaded polymeric micelles with small size for intravenous drug delivery and their inhibitory effect on tumor growth and metastasis in clinically associated 4T1 murine breast cancer. Int J Nanomed 11: 5457-5472.

Dent R, Trudeau M, Pritchard KI, Hanna WM, Kahn HK, Sawka CA, Lickley LA, Rawlinson E, Sun P, Narod SA (2007) Triple-negative breast cancer: clinical features and patterns of recurrence. Clin Cancer Res 13: 4429-4434.

Dreis S, Rothweiler F, Michaelis M, Cinatl J Jr, Kreuter J, Langer K(2007) Preparation, characterisation and maintenance of drug efficacy of doxorubicin-loaded human serum albumin (HSA) nanoparticles. Int J Pharm 341:207–214.

Ding DW, Tang XL, Cao XL, Wu JH, Yuan AH, Qiao Q, Pan J, Hu YQ (2014) Novel self-assembly endows human serum albumin nanoparticles with an enhanced anti-tumor efficacy. AAPS PharmSciTech 15: 213-222.

Fidler IJ (2003) The pathogenesis of cancer metastasis: the 'seed and soil' hypothesis revisited. Nat Rev Cancer 3: 453-458.

Fayaz MS, El-Sherify MS, El-Basmy A, Zlouf SA, Nazmy N, George T, Samir S, Attia G, Eissa H (2013) Clinicopathological features and prognosis of triple negative breast cancer in Kuwait: A comparative/perspective analysis. Rep Pract Oncol Radiother 19: 173-181.

Gelderblom H, Verweij J, Nooter K, Sparreboom A (2001) Cremophor EL: the drawbacks and advantages of vehicle selection for drug formulation. Eur J Cancer 37: 1590-1598.

Gradishar WJ (2006) Albumin-bound paclitaxel: a next-generation taxane. Expert Opin Pharmacother 7: 1041-1053.

Gupta GP, Massagué J (2006) Cancer metastasis: building a framework. Cell 127: 679-695.

Ibrahim NK, Desai N, Legha S Soon-Shiong P, Theriault RL, Rivera E, Esmaeli B, Ring SE, Bedikian A, Hortobagyi GN, Ellerhorst JA (2002) Phase I and pharmacokinetic study of ABI-007, a Cremophor-free, protein-stabilized, nanoparticle formulation of paclitaxel. Clin Cancer Res 8: 1038-1044.

Kaur P, Nagaraja GM, Zheng H, Gizachew D, Galukande M, Krishnan S, Asea A (2012) A mouse model for triple-negative breast cancer tumor-initiating cells (TNBC-TICs) exhibits similar aggressive phenotype to the human disease. BMC Cancer 12: 120.

Kodack DP, Askoxylakis V, Ferraro GB, Fukumura D, Jain RK (2015) Emerging strategies for treating brain metastases from breast cancer. Cancer Cell 27: 163-175.

Kouchakzadeh H, Safavi MS, Shojaosadati SA (2015) Efficient delivery of therapeutic agents by using targeted albumin nanoparticles. Adv Protein Chem Struct Biol 98: 121-143.

Mahamodhossen YA, Liu W, Rong-Rong Z (2013) Triple-negative breast cancer: new perspectives for novel therapies. Med Oncol 30: 653.

Neesse A, Frese KK, Chan DS, Bapiro TE, Howat WJ, Richards FM, Ellenrieder V, Jodrell DI, Tuveson DA (2014) SPARC independent drug delivery and antitumour effects of nab-paclitaxel in genetically engineered mice. Gut 63: 974-983.

Rivolta I, Panariti A, Lettiero B, Sesana S, Gasco P, Gasco MR, Masserini M, Miserocchi G. (2011) Cellular uptake of coumarin-6 as model drug loaded in solid lipid nanoparticles. J Physiol Pharmacol 62: 45-53.

Schnitzer JE, Oh P (1992) Antibodies to SPARC inhibit albumin binding to SPARC, gp60, and microvascular endothelium. Am J Physiol 263: H1872-1879.

Swede H, Gregorio DI, Tannenbaum SH Brockmeyer JA, Ambrosone C, Wilson LL, Pensa MA, Gonsalves L, Stevens RG, Runowicz CD (2011) Prevalence and prognostic role of triple-negative breast cancer by race: a surveillance study. Clin Breast Cancer 11: 332-341.

Srivastava SK, Bhardwaj A, Arora S, Tyagi N, Singh S, Andrews J, McClellan S, Wang B, Singh AP (2015) MicroRNA-345 induces apoptosis in pancreatic cancer cells through potentiation of caspase-dependent and -independent pathways. Br J Cancer 113: 660-668.

Tao K, Fang M, Alroy J, Sahagian GG (2008) Imagable 4T1 model for the study of late stage breast cancer. BMC Cancer 8: 228.

Uematsu T (2011) MR imaging of triple-negative breast cancer. Breast Cancer 18: 161-164.

van Zuylen L, Karlsson MO, Verweij J, Brouwer E, de Bruijn P, Nooter K, Stoter G, Sparreboom A (2001) Pharmacokinetic modeling of paclitaxel encapsulation in Cremophor EL micelles. Cancer Chemother Pharmacol 47: 309–318.

Waugh WN, Trissel LA, Stella VJ(1991) Stability, compatibility, and plasticizer extraction of taxol (NSC-125973) injection diluted in infusion solutions and stored in various containers. Am J Hosp Pharm 48:1520–1524.

Wartlick H, Spänkuch-Schmitt B, Strebhardt K, Kreuter J, Langer K(2004) Tumour cell delivery of antisense oligonuclceotides by human serum albumin nanoparticles. J Control Release 96:483–495.

Wang HB (2008) Studies on anti-tumor activities and its mechanisms of Lx2-32c, one new taxane. Dissertation. Beijing: Chinese academy of medical sciences & Peking union medical college.

Wang HB, Li HY, Zuo MX, Zhang Y, Liu H, Fang WS, Chen XG (2008a) Lx2-32c, a novel taxane and its antitumor activities in vitro and in vivo. Cancer Lett 268: 89-97.

Wang HB, Li HY, Fang WS, Chen XG (2008b) Inhibiting effect of Lx2-32c, one taxane derivant, on the proliferation of human ovary A2780 cells. Chin New Drug J 17: 833-836 (in Chinese).

Wang HB, Zhang JQ, Lv GY, Ma JB, Ma PK, Du GY, Wang ZL, Tian JW, Fang WS, Fu FH (2014) Preparation, pharmacokinetics, biodistribution, antitumor efficacy and safety of Lx2-32c-containing liposome. PLoS One 15: e114688.

Wan X, Zheng XY, Pang XY, Zhang ZM, Jing T, Xu W, Zhang QZ (2015) The potential use of lapatinib-loaded human serum albumin nanoparticles in the treatment of triple-negative breast cancer. Int J Pharm 484: 16-28.

Wang CH, Xiang R, Zhang XZ, Chen YX (2015) Doxycycline inhibits leukemic cell migration via inhibition of matrix metalloproteinases and phosphorylation of focal adhesion kinase. Mol Med Rep 12: 3374-3380.

Xiao X, Wu J, Trigili C, Chen H, Chu JW, Zhao Y, Lu P, Sheng L, Li Y, Sharom FJ, Barasoain I, Diaz JF, Fang WS (2011) Effects of C7 substitutions in a high affinity microtubule-binding taxane on antitumor activity and drug transport. Bioorg Med Chem Lett 21: 4852-4856.

Xu M, Bu LM, Wu K, Lu LG, Wang XP (2015) Rapamycin inhibits the proliferation of SW1990 pancreatic cancer cell. Eur Rev Med Pharmacol Sci 19: 3072-3079.

Zhang Y, Huo MR, Zhou JP, Zou AF, Li WZ, Yao CL, Xie SF (2010) DDSolver: an add-in program for modeling and comparison of drug dissolution profiles. AAPS J 12: 263-271.

Zhou Q (2012) Studies on anti-drug-resistance activities and mechanisms of action of Lx2-32c, a novel taxane. Dissertation. Beijing: Chinese academy of medical sciences & Peking union medical college.

Zhou Q, Li Y, Jin J, Lang LW, Zhu ZX, Fang WS, Chen XG (2012) Lx2-32c, a novel taxane derivative, exerts anti-resistance activity by initiating intrinsic apoptosis pathway in vitro and inhibits the growth of resistant tumor in vivo. Biol Pharm Bull 35: 2170-2179.